JOURNAL OF PROPULSION AND POWER
Vol. 10, No. 1, Jan.–Feb. 1994

Installed F/A-18 Inlet Flow Calculations at a High Angle of Attack

James E. Bruns* and C. Frederic Smith†
Sverdrup Technology, Inc., Brook Park, Ohio 44142

One of the goals of the high alpha technology program (HATP) is to accurately predict the inlet performance for aircraft operating at extreme attitudes (α = 60 deg, β = 10 deg). In this article, the numerical results for three cases are presented. The cases studied are full scale, 19.78% model scale at design mass flow, and model scale at a reduced mass flow. The effects of Reynolds number on the predicted flowfield is demonstrated with the model and full scale calculations. The inlet mass flow is reduced 25% to investigate the effect mass flow rate has on the flow entering the inlet and on the inlet duct performance. All cases are at 30-deg angle of attack and 0-deg yaw. Surface static pressures along the forebody and under the leading edge extension (LEX) agreed well with the data for all three cases. The predicted inlet recoveries obtained for full scale and model scale Reynolds numbers were very similar. The predicted inlet recoveries were lower than data. This discrepancy may be partly due to poor inlet lip definition and grid resolution. The predicted inlet recovery for the reduced mass flow rate case was significantly higher than the design mass flow case. The reduction of inlet mass flow rate had a small effect on the external flowfield. The choice of the turbulence model length scale has a significant impact on the position of the windward side LEX vortex.

Introduction

ONE of the goals of the high alpha technology program is to accurately predict the aerodynamics of aircraft operating at extreme attitudes (α = 60 deg, β = 10 deg). As part of this program, the use of external aerodynamics including thrust vectoring control systems and vortex flow control are being examined. In addition, the effects of high angle of attack and yaw flight conditions on flow within the F/A-18 inlet duct are being studied numerically and experimentally. Details of this cooperative program are contained in Ref. 1. The effects of rate will be considered for the flight tests only. The F/A-18 aircraft has experienced engine stalls at high angles of attack and yaw flight conditions which were outside of the flight envelope. At these flight conditions, high angular rates were also present. Future fighter aircraft will be designed to operate routinely in this flight regime. Therefore, it is essential that an understanding of the inlet flowfield at these flight conditions be obtained. Due to the complex interactions of the fuselage flowfield and the inlet flowfield, a study of the flow within the inlet must also include the external effects. Past calculations of flow about the F/A-18 have not included the inlet and ramp.[2,3] These features are usually fared over and assumed not to influence the external flowfield significantly. However, the effects from the upstream forebody must be included in order to provide the proper inflow conditions to the inlet duct.

Full Navier-Stokes calculations on the installed F/A-18 inlet at 30-deg angle of attack, 0-deg yaw, and a freestream Mach number of 0.2 have been obtained in this study using a full Navier-Stokes code with an algebraic turbulence model. In order to account properly for the external effects, the forebody, LEX, ramp, and wing were included with inlet geometry as shown in Fig. 1. The diverter, LEX slot, and leading-edge flap were not included due to insufficient geometry definition. The calculations are compared to data. In particular, data for the inlet flowfield are very limited. One of the objectives of the CFD effort is to aid in the interpretation of future experimental results. The numerical simulations can provide information concerning regions of the flowfield that are not measured.

This article is divided into several sections. Various aspects of the numerical modeling will be presented. This will include a brief description of the Navier-Stokes code and boundary conditions used. A brief discussion of the geometry used and the computational grid is also included in this section. The results for the three cases studied are presented next. Flow features common to the three solutions are discussed first, followed by a discussion of the differences observed between the cases. Computational issues are discussed next which include convergence criteria and turbulence modeling. The report is completed with a section stating conclusions and recommendations.

Numerical Modeling

In this section, several aspects of simulating the flow around and within the F/A-18 inlet are presented. The flow analysis code is briefly discussed. A discussion of the geometry used and the computational grid is presented. A description of the boundary conditions implemented concludes this section.

PARC3D Code

The PARC3D code[4] solves the full three-dimensional Reynolds-averaged Navier-Stokes equations in strong conserva-

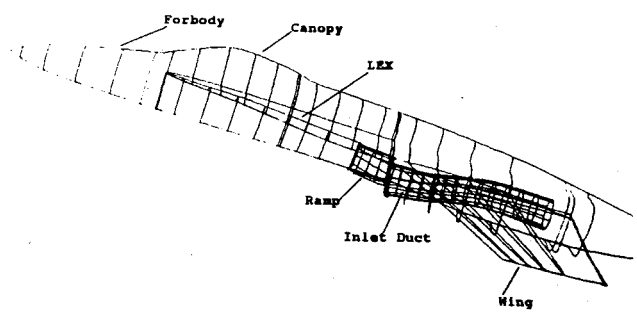

Fig. 1 F/A-18 Components diagram.

Received May 15, 1992; presented as Paper 92-3175 at the AIAA/SAE/ASME/ASEE 28th Joint Propulsion Conference, Nashville, TN, July 6–8, 1992; revision received May 13, 1993; accepted for publication June 3, 1993.

*Lewis Research Center Group; currently at Lehr Precision, Inc., Cincinnati, OH.

†Supervisor, Propulsion Aerodynamics Section, Lewis Research Center Group. Senior Member AIAA.

tion form using the Beam and Warming approximate factorization scheme to obtain a block tridiagonal system of equations. Pulliam's scalar pentadiagonal transformation provides for an efficient solver. The code uses the Baldwin-Lomax turbulence model.[5] The implicit scheme uses central differencing with artificial dissipation to eliminate oscillations in the solution associated with the use of central differences. This code allows for the use of multiple grid blocks. Trilinear interpolation[6] is used to transfer information at the grid block interfaces.

Geometry and Computational Grid

The grid used to model the F/A-18 in this study was a very important factor in obtaining a good solution. Accurate modeling of the geometry and judicious clustering of grid points is needed for a correct numerical solution and an economical computation. The complex multiblock grid used for these calculations was created with the GRIDGEN grid generation system of codes.[7] This grid generator has proven to be very effective in creating complex multiblock grids. Due to the complex interactions between the fuselage flowfield and the inlet flowfield, the forebody, fuselage, LEX, ramp, and wing were all included in the grid. The horizontal tail, vertical tail, and the nozzle were not modeled because of their minimal effects on the inlet flowfield. The wing leading-edge flap, which is deflected down 34 deg when the aircraft is at 30-deg angle of attack, was modeled undeflected. A pair of vortex generators which are positioned approximately halfway downstream in the inlet duct were also not modeled due to their small size.

The blocking structure used for the F/A-18 consists mainly of C-grids wrapped around the fuselage, in the crossflow plane. The entire F/A-18 blocking structure can be seen in Fig. 2. The blocks were created such that the blocks under the LEX could be run viscous, while the blocks over the LEX could be run Euler. This was done because it was felt that the viscous effects above the LEX did not significantly affect the flow into the inlet. This also decreased the required number of grid points, and therefore, the run times. The entire computational grid contained approximately 1.1 million points, of which 670,000 were in the viscous regions. Blocks were extended approximately one body length away from the surface in order to minimize the effects of the freestream boundary condition on the solution near the inlet. The inlet block contains an O-grid extending from the inlet lip to the compressor face. The inlet duct grid block had dimensions of 66, 50, and 49 points in the streamwise, circumferential, and radial directions, respectively. The y^+ values of the first off-surface grid points in the inlet duct varied from approximately 4 at the entrance to 2 at the compressor face.

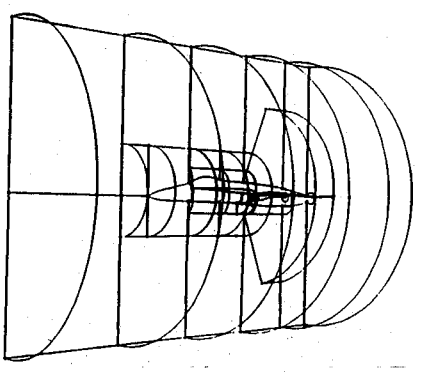

Fig. 2 Block structure of the computational grid.

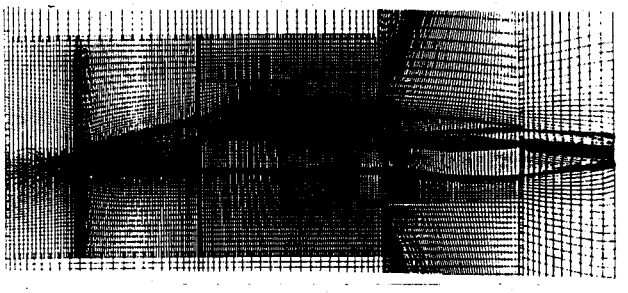

Fig. 3 Plane-of-symmetry view of computational grid.

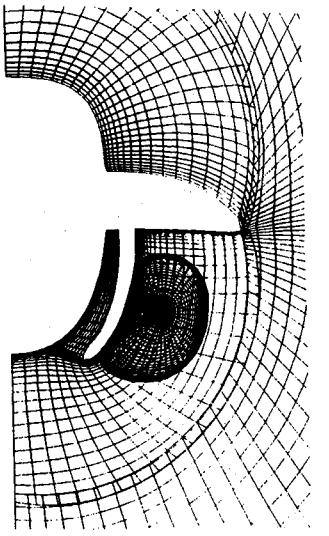

Fig. 4 Cross-sectional view of grid ahead of the inlet entrance.

The grid on the symmetry plane and on the F/A-18 surface can be seen in Fig. 3. An axial cut of the grid ahead of the inlet is shown in Fig. 4.

Boundary Conditions

The far-field-type boundary conditions were imposed along the outer computational boundaries. This type of condition uses a one-dimensional Riemann invariant to maintain the freestream flow conditions. Along the windward side of the airframe, no-slip, adiabatic conditions are specified. Along the leeward side of the aircraft, slip wall and inviscid flow are specified. The static pressure at the inlet duct exit was adjusted to obtain the equivalent experimental corrected mass flow based upon total pressure at the engine face plane obtained from an average of 40 total pressures in a configuration of 8 equally spaced legs with 5 equal area total pressure locations per leg. Symmetry conditions were assumed along the centerline of the aircraft. Trilinear interpolation is used to transfer data between the grid blocks.

Results

The results presented cover several areas. A brief discussion of three cases studied is presented. This is followed by a discussion of the external flowfield calculations and comparisons of predicted to measured surface static pressures. The details of the inlet flowfield are presented next with comparisons of predicted compressor face total pressures with data. Differences in the three cases are discussed in the final subsection.

Case Studies

Three cases were run to explore the different aspects of the F/A-18 inlet flowfield at 30-deg angle of attack. The cases are shown in Table 1. Case 1 was run at a 19.78% wind-tunnel model scale with the design inlet mass flow. It was run to simulate the wind-tunnel test at design conditions. Case 2 was also run at 19.78% wind-tunnel model scale, but the inlet corrected mass flow was reduced 25%. This case was run to determine the effects of the inlet mass flow rate on the inlet performance and on the external flowfield near the inlet entrance. In previous wind-tunnel tests, which focused on external aerodynamics, flow-through inlets were used which

Table 1 Case studies

Case	1	2	3	Data
Mach number	0.2	0.2	0.2	0.2
α	30	30	30	33
R_e (10^6)	3.26	3.26	16.48	3.16
Mdot (cor)	5.87	4.30	150.0	5.29
Velocity ratio	2	1.5	2	1.9
Mass flow ratio	0.82	0.60	0.82	0.79

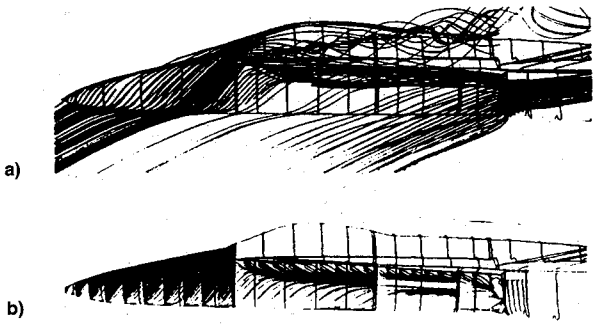

Fig. 5 a) Predicted particle trajectories ahead of inlet and b) surface particle trajectories along the forebody and under the LEX.

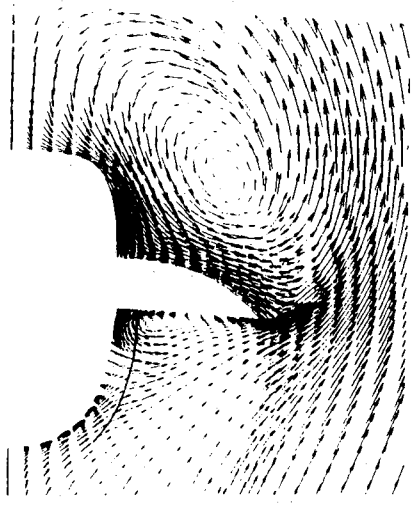

Fig. 6 Flowfield vectors at the ramp leading edge.

produce a significantly lower than design mass flow rate. The rates obtained with flow-through inlets may be less than the reduced flow rate case studied in this article. Case 3 was run with a Reynolds number which corresponds to a full-scale aircraft, and it was used to determine the scaling effects on the solution. The data[8] were obtained using a 19.2% scale model of the F/A-18 aircraft. All the numerical cases produced some results which were similar. Therefore, case 1 will be used as a representative solution to discuss the features which were common to all three cases. The differences between the results of each case will be discussed in a later section.

The grid used in this study is considered preliminary. It was generated based upon intuitive knowledge of the flowfield. In addition, certain parts of the aircraft, such as around the highlight of the inlet lip, did not have adequate geometric definition. Based upon the present results and an improved geometry data base, a revised grid will be generated and updated solutions obtained.

External Flow Results

At 30-deg angle of attack, a vortex is formed underneath the LEX as can be seen in Fig. 5a. In addition, another vortex is formed along the leeward side of the aircraft originating at the beginning of the LEX-fuselage intersection. The windward vortex is generated when the flow impinges on the bottom of the LEX and moves inboard towards the LEX root. The flow then moves down the fuselage until it reaches a separation point. The separation line is visible in the surface particle traces of Fig. 5b. This vortex is ingested by the inlet.

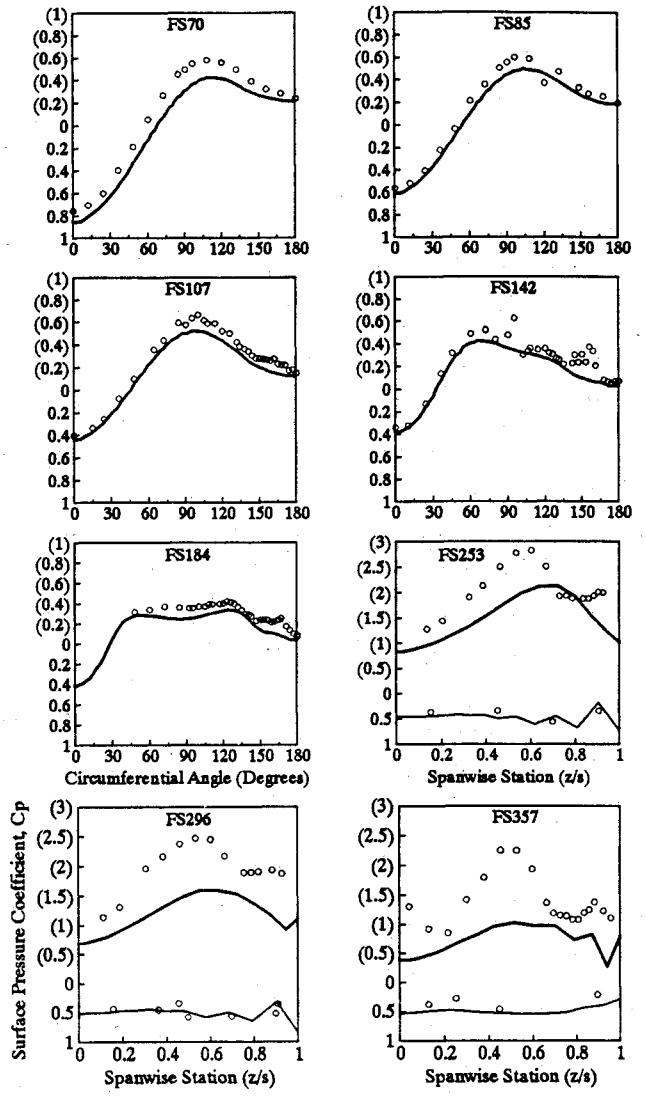

Fig. 7 Surface static pressures along fuselage and LEX.

The windward and leeward side vortices can be seen in the velocity vectors in Fig. 6. The windward vortex is at the leading edge of the ramp in this figure. Since the geometry for the diverter and the slot through the LEX were not available, a simple H-grid was used to model the flow behind the ramp with ambient pressure specified at the block exit. The effects on the vortex of ambient pressure being imposed at the exit of the block behind the ramp is not yet known. The vortex is finally ingested into the inlet, which will be discussed further in a later section.

There is a significant amount of external data which could be used to gain confidence in the predicted external flowfield. Predicted static pressure distributions at five axial stations on the nose and three axial stations on the LEX of the 19.78% scale model at design mass flow (case 1 in Table 1) were compared with flight test data obtained by Fisher et al.[9] The comparisons can be seen in the plots of Fig. 7. Zero deg corresponds to the bottom, windward side of the aircraft, and 180 deg corresponds to the top, leeward side of the aircraft. Comparisons are very good at stations on the nose, fuselage station (F.S.) 70 through F.S. 184. The only discrepancy is the failure to pick up the vortex which produced the pressure decreases at F.S. 142 at 150 deg and F.S. 184 at 180 deg. This failure was probably due to the coarsened circumferential grid on the top of the nose or to the coarse Euler grid above the

LEX affecting the flow upstream on the nose. The comparisons of the data on the LEX, F.S. 253 through F.S. 357, show good agreement under the LEX, but the calculated pressures above the LEX are well below the experimental values. This is probably due to the coarse Euler grid being used above the LEX. The flowfield above the LEX, however, does not appear to have a significant impact on the inlet flowfield.

The predicted surface pressure distributions obtained for the full-scale case were the same as the distributions obtained for the 19.78% scale model. Therefore, it appears that the Reynolds number effects for the external flowfield are negligible for this model scale.

Inlet Flowfield Results

The normalized total pressures at different stations through the inlet are shown in Fig. 8. The normalized total pressure is the ratio of the local total pressure to the freestream total pressure. It can be seen from the total pressure contours near the inlet entrance, that a thick boundary layer has formed, except along the inboard wall of the inlet. The boundary layer is small there because the inside portion of the inlet meets the ramp at the inlet entrance and the flow is not turning around the inlet lip in this region. From examining the predicted Mach number distributions in the inlet entrance region, the highest levels are approximately 0.8, which indicates that shock-boundary layer interactions are not the source of the thickening boundary layers. However, downstream in the inlet throat region there is a small region of sonic flow in the lower inboard corner of the duct. There is a rapid rise and drop in static pressure around the inlet highlight which is shown in Fig. 9. Locally, there is an 11% total pressure overshoot which is diminished to 2% in the flowfield away from the wall. The total pressure overshoots are discussed in a later section.

The flow experiences a rise in static pressure along the cowl prior to moving around the lip highlight, which is followed by a rapid drop in static pressure. The rise in static pressure is a contributor to the thickening boundary layer. Pressure fluctuations are also present due to inadequate surface resolution which may also contribute to the predicted thickening boundary layers. The discrepancy in the static pressure at the highlight is due to the fuselage and inlet grids not being coincident. The numerical results also indicate the presence of flow separation along the lower portion of the lip. The location of the grid block interfaces along the lip highlight may also be contributing to the thickening boundary layer along the lip surface.

The F/A-18 inlet duct bends inboard and upward along its length. The region of low total pressure in the lower inboard region of the inlet is a result of the inlet duct vortical flow and streamwise separated flow within the vortex. This separated flow region may not be present in the actual flowfield and possibly be the result of poor lip definition and/or the lack of vortex generators in the numerical model. At the compressor face the total pressure distribution is actually due to two vortices. These vortices can be seen in the vorticity contours in Fig. 10. The clockwise rotating vortex, positioned in the bottom inboard region of the inlet, may be due to the inflection of the duct to accommodate the nose landing gear and/or the absence of the pair of vortex generators in the numerical simulation. The counterclockwise rotating vortex near the duct center is a result of the ingestion of the vortical flow produced under the LEX. The ingested vortex appears to have a smaller contribution to the overall flowfield distortion at the inlet duct exit than the inlet duct vortex.

Limited experimental data for the internal inlet duct flow exists for the installed F/A-18 inlet at 33-deg angle of attack. Some data produced by Northrop in the late 1970s and early 1980s was obtained for comparison.[8] The calculated and experimental stagnation pressures at the compressor face are compared in Fig. 11. For this figure only, these pressures are presented as the percent over or under the rake-averaged total pressure at the engine face. Qualitative comparisons show the low and high total pressure regions are in similar locations. However, the experimental data show somewhat higher levels overall. The presence of the ingested vortex is not seen in the data. This may be due to the vortex position being near the center of the duct in the predicted results and not being resolved by the rakes. The experimental data indicates that the

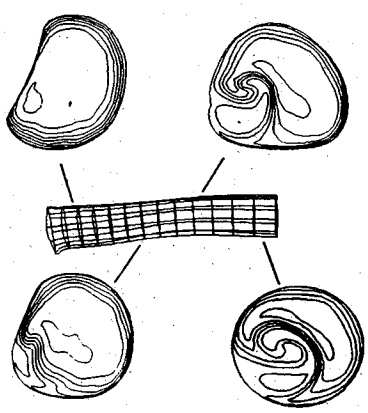

Fig. 8 Normalized total pressure contours at four stations inside inlet duct.

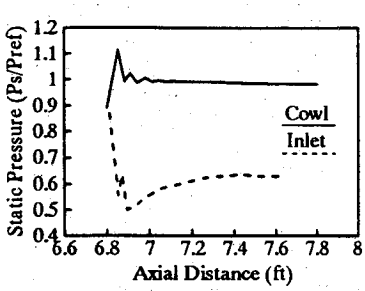

Fig. 9 Surface static pressure distribution along lower lip highlight.

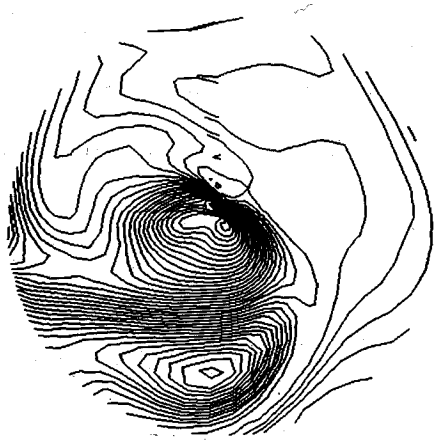

Fig. 10 Vorticity contours at the inlet duct exit.

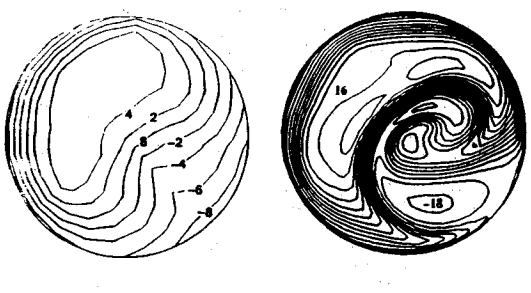

Fig. 11 Normalize total pressure contours at inlet duct exit (% above or below mean P_T).

predicted secondary flowfield losses are too large, and therefore, effects of the ingested vortex on the flowfield distortion may be more significant if the predicted secondary flowfield distortions are reduced. The very low values of predicted total pressure are partly attributable to streamwise flow separation in this region.

In the actual inlet duct one pair of counter-rotating vortex generators are placed in the bottom of the inlet duct. They were installed to alleviate the possible streamwise separation which might occur at the inflection on the inlet wall, due to the landing gear placement. Because of their size (approximately 1 in., full scale) and number, they may not have a significant effect on the vortical flow. However, since their position is ahead of the predicted streamwise flow separation, they may be a contributing factor in the discrepancies seen between the data and the numerical results.

Comparisons of Different Cases

The effects of scale and mass flow rate will be discussed in this section. Since the full scale results were very similar to the model scale, only the model scale and reduced flow rate results will be shown. The effect of reducing the inlet mass flow rate is to cause the ingested vortex to move slightly outboard. A comparison of the model scale to full scale cases at design mass flow rate indicates the position of the ingested vortex at the inlet entrance is very similar.

The change in inlet corrected mass flow between cases 1 and 2 had a significant effect on the inlet flowfield (see Table 1 for definition of cases). The difference in scale (Reynolds number) between cases 1 and 3 did not produce significant changes in the inlet flowfield. Comparisons of inlet recoveries, total pressure distortions, and compressor face Mach numbers are given in Table 2. All values were obtained from averaging data at positions corresponding to an equal area 40 probe rake. The predicted total pressure recoveries are somewhat lower than the measured values[8] shown in Table 2. Also, the predicted distortions are higher than the data. This implies that the secondary flowfield losses are overpredicted, which is consistent with the previously discussed comparisons of total pressures using 40 probe rakes. Poor lip definition may be a contributing factor to the higher losses predicted. Another contributing factor is the presence of reverse flow within the vortex.

Table 2 Values at the compressor face

Case	1	2	3	Data
Inlet recoveries	88%	92%	86%	94.5%
Distortion	0.3	0.18	0.32	0.18
Mach number	0.46	0.34	0.48	0.45

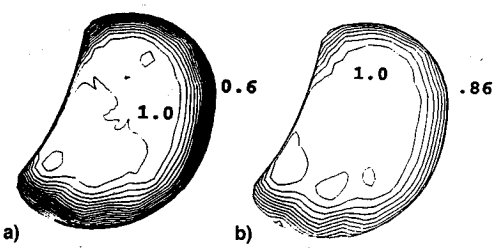

Fig. 12 Normalized total pressure contours at inlet entrance: a) model scale, design mass flow and b) model scale, reduced mass flow.

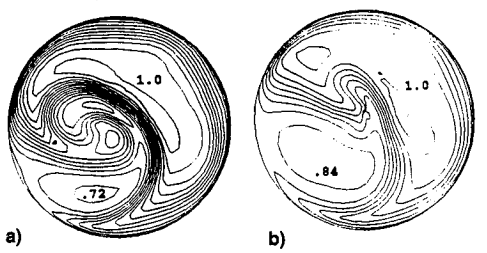

Fig. 13 Normalized total pressure contours at the inlet exit: a) model scale, design mass flow and b) model scale, reduced mass flow.

From case 1 to case 2, the inlet recoveries increased by 4%, and the distortions decreased by 40% with the 25% reduction of inlet mass flow. The increase in inlet performance was due, in part, to the decrease in the losses generated at the inlet lip. With a velocity ratio of 1.5 instead of 2, the flow is accelerated less and is not turned as much around the inlet lip. This means there is a higher energy flow for case 2 at the beginning of the inlet as shown by the total pressures in Fig. 12. The velocity flow ratio is defined as the ratio of the mass-weighted velocity at the inlet entrance to the velocity calculated using freestream conditions. The full scale normalized total pressure contours at the inlet entrance are very similar to the model scale design mass flow case. The normalized total pressures at the compressor face are shown in Fig. 13. The total pressure contours have similar shapes, but the levels are higher for the reduced mass flow rate case. Another contributor to the increase in the predicted recovery is the 26% reduction in the duct exit Mach number. The lower flow velocities in the duct will result in a decrease in the total pressure losses. The mass flow ratios shown in Table 1 indicate that the inlet is nearing choked conditions at design mass flow. The mass flow ratio is defined as the actual mass flow rate divided by the isentropic choked mass flow rate at the inlet entrance. The calculated effects of velocity ratio on inlet performance are consistent with experimental data.[8] The data for 33-deg angle of attack indicates that at design mass flow the inlet recovery is 94.5%, and at 25% reduced mass flow the recovery has increased to 98%. This increase in the experimental recovery is very close to the computed results. The change in Reynolds number between cases 1 and 3 did not have a significant effect on the compressor face distortions. This lends confidence that the future wind-tunnel tests will accurately simulate the flowfields that occur at flight conditions at a Mach number of 0.2. The predicted compressor face total pressure contours for design mass flow rate full scale and model scale cases are very similar. The value of normalized total pressure for the reduced mass flow case within the vortex is much higher than the design flow rate cases.

The total pressure contours shown in Fig. 12 indicate regions of 2% total pressure overshoots. This is attributed to the grid block interface surfaces joining along the inlet lip highlight and the poor definition of this region. Along this surface the flow is undergoing very rapid changes which may not be modeled adequately with the present grid. Information is transferred between grid blocks using trilinear interpolation, which is not a conservative scheme. Therefore, performing linear interpolations in regions of rapid flow changes may produce some errors in conservation properties. This may also contribute to the thickening of the boundary layers along the lip surface as previously discussed. The overshoots in normalized total pressure are reduced to 1% in small regions of the flowfield at the inlet duct exit. These regions are not shown in the duct exit flowfield contours since they were limited to small regions of the flow and to provide for easier interpretation of the results. The use of a C-grid around the lip should alleviate this problem by eliminating the interface junction lying along the lip highlight and improved surface resolution.

Numerical Issues

In this section, various issues regarding the validation of the computational results in light of the limited experimental data available will be discussed. The convergence of the internal and external flowfield solutions are presented. The effects on the solution due to changes in the algebraic turbulence model are discussed.

Solution Convergence

The residual levels for this problem dropped between 4–6 orders of magnitude, depending upon which grid block the

residuals are associated with. Therefore, other parameters must be looked at to determine the convergence of the solution. For internal flows, the error in mass flow rate or continuity is a very useful integrated quantity. This was used to evaluate the convergence of the inlet flowfield solution. The error was within 1% throughout the duct, although the inlet flowfield exhibited some unsteadiness. For the external flowfield, the lift and drag coefficients were used. Due to the close proximity of the external outer flow boundaries to the aircraft and geometric modeling approximations made, the absolute values were in error when compared to existing experimental data. However, the changes in these values as the solution is iterated should give an indication of the convergence of the external flowfield.

It was found that the lift and drag coefficients were unsteady and varied by 10–15% as the solution was iterated. Most of this variation is attributed to the wing as a result of examining the forces generated for each grid block containing a surface. This unsteadiness in the lift and drag does not appear to affect the flow entering the inlet. The predicted surface static pressures along the forebody and LEX were steady with the exception of F.S. 70 which exhibited small variations as the solution was iterated. The second- and fourth-order dissipation coefficients were set at values of 0.25 and 0.64, as recommended in the PARC3D manual. Due to the complexity of the calculations, experiments with different values were not done.

Turbulence Modeling

It was found that restricting the distance from the wall for the turbulence length scale search had a significant effect on the flowfield. In particular, the windward side vortex from the forebody/LEX junction was not ingested when the length scale search was unrestricted. However, results obtained for vortical flows in ducts[10] indicated that improvements in the solution were obtained by restricting the length scale search to regions close to a wall. The restrictions were implemented by restricting the length scale search range in terms of grid indices to those within the boundary layers. The effects of crossflow were accounted for by using only the component of vorticity normal to the flow direction to determine the turbulent viscosity. This is discussed in Ref. 10. When this approach was applied to this F/A-18 forebody flowfield, the external vortex was ingested by the inlet. Due to the validation of this type of turbulence modeling on similar vortical flow problems, there is some confidence in the ingested vortex being the proper simulation. This example highlights the use of the results obtained from simple or fundamental flow problems being incorporated into complex simulations, and providing confidence in the solution when data is not available.

Conclusions and Recommendations

Calculations were presented for the flowfield within an F/A-18 inlet at 30-deg angle of attack. These calculations were performed ahead of tests in order to provide guidance for the interpretation of experimental data and insight into the flowfield physics. The grid used is considered a first attempt to model the internal and pertinent external flowfields. In order to provide the proper inflow conditions, much of the upstream external flowfield had to be included by modeling the forebody, LEX, wing, and ramp. The external flowfield predicted for all three cases was very similar. The ingested vortex moved slightly outboard when the inlet mass flow rate was reduced. The position of the ingested vortex was similar for the model scale and full scale cases at design mass flow. The model and full scale calculations provided similar results for the inlet duct flowfield at design mass flow. The model scale reduced mass flow case provided lower losses than the design mass flow cases. These predicted trends are similar to the data that is available. The predicted total pressure recoveries are low when compared to data. This may be attributed to poor lip definition and grid resolution. The ingested vortex does not appear to be the main contributor to losses in the inlet, although it may be of more significance since the predicted secondary flowfield losses are larger than the experimental data. The effects of Reynolds number for the scale model being used appear to be small, and therefore, the wind-tunnel tests should model the in-flight flow conditions reasonably well. The choice of length scale for the turbulence model had a significant impact on the position of the windward side LEX vortex.

There are several areas for improvement for future calculations. The diverter and slot through the LEX should be modeled to provide more realistic conditions. Improved external lip definition from the data base should also be incorporated. Future studies should use a C-grid around the lip to better define its surface and about the forebody. The leading-edge flap should also be deflected and modeled with an embedded C-grid in order to provide a more accurate model of the geometry near the inlet entrance.

Acknowledgments

Support of this work by the NASA Lewis Research Center of the National Aeronautics and Space Administration and under Contract NAS3-25266 is gratefully acknowledged. The interest shown by Project Manager, Richard R. Burley, is particularly appreciated. In addition, the authors thank Raymond R. Cosner of McDonnell Aircraft Company in St. Louis, MO, for his help in obtaining the F/A-18 aircraft geometry data base. The authors would also like to thank Susan Zeleznik for her assistance in the preparation of the text and figures for this article.

References

[1]Burley, R. R., Anderson, B. H., Smith, C. F., and Harloff, G. J., "High Alpha Inlets," Aeropropulsion '91, NASA CP 10063, March 1991, pp. 5-1–5-14.

[2]Ghaffari, F., Bates, B. L., Luckring, J. M., Thomas, J. L., and Biedron, R. T., "Navier-Stokes Solutions About the F/A-18 Wing-LEX-Fuselage Configuration with Multi-Block Structured Grids," AIAA Paper 91-3291, Sept. 1991.

[3]Gee, K., Tavella, D., and Schiff, L. B., "Computational Optimization of a Pneumatic Fuselage Forebody Flow Control Concept," AIAA Paper 91-3249, Sept. 1991.

[4]Cooper, G. K., and Sirbough, J., "The PARC Distinction: A Practical Flow Solver," AIAA Paper 90-2002, July 1990.

[5]Baldwin, B. S., and Lomax, H., "Thin Layer Approximation and Algebraic Turbulence Model for Separated Turbulent Flows," AIAA Paper 78-257, Jan. 1978.

[6]Stokes, M. L., and Kneile, K. L., "A Search/Interpolation Algorithm for CFD Analysis," World Congress on Computational Mechanics, Univ. of Texas, Austin, TX, Sept. 1986.

[7]Steinbrenner, J. P., Chawner, J. R., and Fouts, C. L., "The Gridgen 3-D Multiple Block Grid Generation System," Wright Research and Development Center TR-90-30222, Wright-Patterson AFB, OH, 1991.

[8]Amin, N. F., Hollweger, D. J., Franks, W. J., De La Vega, E. G., Yamada, M., and Tsukahira, T. W., "AEDC Series 1 F/A-18, .192 Scale Inlet Analysis Report," Northrop Corp., Aircraft Div., NOR 77-310, Hawthorne, CA, May 1977.

[9]Fisher, D. F., Banks, D. W., and Richwine, D. M., "F/A-18 High Alpha Research Vehicle Surface Pressures: Initial In-Flight Results and Correlation with Flow Visualization and Wind-Tunnel Data," NASA TM 101724, 1990.

[10]Sirbaugh, J. R., and Reichart, B. A., "Computation of a Circular-to-Rectangular Transition Duct Flow Field," AIAA Paper 91-1741, June 1991.